
Article:
Wood, W.H.J., MacGregor-Chatwin, C., Barnett, S. et al. (5 more authors) (2018) Dynamic thylakoid stacking regulates the balance between linear and cyclic photosynthetic electron transfer. Nature Plants, 4. pp. 116-127. ISSN 2055-026X

https://doi.org/10.1038/s41477-017-0092-7

Dynamic thylakoid stacking regulates the balance between linear and cyclic photosynthetic electron transfer

William H. J. Wood[a], Craig MacGregor-Chatwin[a], Samuel F. H. Barnett[a], Guy E. Mayneord[a], Xia Huang[a], Jamie K. Hobbs[b], C. Neil Hunter[a] and Matthew P. Johnson[a*]

[a]Department of Molecular Biology and Biotechnology, University of Sheffield, Firth Court, Western Bank, Sheffield, S10 2TN, United Kingdom.
[b]Department of Physics and Astronomy, University of Sheffield, Hicks Building, Hounsfield Road, Sheffield, S3 7RH, United Kingdom.
*Corresponding Author

Upon transition of plants from darkness to light the initiation of photosynthetic linear electron transfer (LET) from H_2O to $NADP^+$ precedes the activation of CO_2 fixation, creating a lag period where cyclic electron transfer (CET) around photosystem I (PSI) has an important protective role. CET generates ΔpH without net NADPH formation, preventing over-reduction of PSI via regulation of the cytochrome *b*$_6$*f* (cyt*b*$_6$*f*) complex and protecting PSII from over-excitation by inducing non-photochemical quenching (NPQ). The dark-to-light transition also provokes increased phosphorylation of light-harvesting complex II (LHCII). However, the relationship between LHCII phosphorylation and regulation of the LET/ CET balance is not understood. Here we show that the dark-to-light changes in LHCII phosphorylation profoundly alter thylakoid membrane architecture and the macromolecular organisation of the photosynthetic complexes, without significantly affecting the antenna size of either photosystem. The grana diameter and number of membrane layers per grana are decreased in the light while the number of grana per chloroplast is increased, creating a larger contact area between grana and stromal lamellae. We show that these changes in thylakoid stacking regulate the balance between LET and CET pathways. Smaller grana promote more efficient LET by reducing the diffusion distance for the mobile electron carriers plastoquinone (PQ) and plastocyanin (PC), while larger grana enhance the partition of the granal and stromal lamellae PQ pools, enhancing the efficiency of CET and thus photoprotection by NPQ.

Introduction

When dark adapted plants are illuminated, they do not immediately commence CO_2 fixation at maximal rates[1]. Rather an induction period generally lasting several minutes is observed. The lag period is thought to reflect the autocatalytic build-up of the chloroplast 3-phosphoglycerate (3-PGA) pool in the Calvin-Benson Cycle to steady state levels[1,2]. Thus, the turnover of NADPH and ATP is initially limited by the low concentration of 3-PGA leading to a transient over-reduction of the stroma[1,2]. Autocatalysis is associated with a higher demand for ATP since initially all the glyceraldehyde-3-phosphate (GAP) is regenerated into ribulose-1,5-bisphosphate (RuBP) rather than a proportion (1/6) being exported from the chloroplast, as during the steady state. This raises the required ATP/ NADPH ratio from 1.5 to 1.6[1]. The reduction of the stroma and increased ATP requirement coincide with a higher rate of cyclic electron transfer (CET) during induction[3,4]. CET cycles electrons from the PSI acceptor side back to PQ, cyt*b*$_6$*f* and PC thereby forming ΔpH and ATP without net NADPH production, modulating the ATP/NADPH ratio to meet metabolic demand[5,6]. CET plays an important role during induction; it allows electrons to be recycled since $NADP^+$ is limiting and thereby allows ΔpH generation for downregulation of PSII by NPQ, protection of PSI from over-reduction by slowing the turnover of the cyt*b*$_6$*f* complex and for the additional ATP synthesis required for autocatalysis[7-9].

Two pathways of CET exist in plants involving the Proton Gradient Regulation (PGR5/PGRL1) and the NADPH dehydrogenase-like (NDH) complexes[5,6]. The PGR5/ PGRL1 pathway is the major contributor to CET in *Arabidopsi*s and spinach, and mutants lacking either protein show lower ΔpH levels, reduced electron transfer capacity in moderate and high light and increased susceptibility to photo-oxidative stress particularly in fluctuating light[7-9]. Debate continues as to the exact role played by PGR5/ PGRL1 in CET. In one view PGR5/ PGRL1 is suggested to be an antimycin A-sensitive ferredoxin- PQ oxidoreductase[8]. Alternatively, it has been proposed that PGR5/PGRL1 may influence CET and indeed LET via regulation of the cyt*b*$_6$*f* and ATP synthase complexes[7,10]. The other CET pathway involves the NDH complex, a large multi-subunit ferredoxin-PQ oxidoreductase that can also pump protons directly to the thylakoid lumen[11] and seems to be particularly important under low light conditions[12].

Proper activation of CET requires 'redox poise' i.e. the maintenance of a pool of relatively oxidised PQ to accept electrons from the PSI acceptor side under conditions where PQ should be largely reduced[4,5]. How this can be achieved is a matter of some debate. In the green alga *Chlamydomonas* PGRL1 forms a supercomplex with cytb_6f and PSI, which could trap a sequestered pool of oxidised PQ[13,14], but in plants no such complex has been found. Alternatively, it has been suggested that thylakoid membrane stacking leads to the isolation of separate PQ pools in the grana and stromal lamellae regions that only slowly equilibrate[15,16]. Thylakoid structure is influenced by the phosphorylation levels of PSII and LHCII, which regulate the surface charges of these complexes and so the cation dependency of stacking[17]. Phosphorylation of LHCII and PSII is controlled by the STN7 and STN8 kinases, which have some overlap in their specificity[18,19]. STN7 phosphorylates LHCII subunits Lhcb1 and 2 and the PSII CP43 subunit, while the STN8 kinase phosphorylates PSII D1, D2 and CP43 subunits[18,19]. The PBCP and TAP38 phosphatases desphosphorylate the PSII and LHCII subunits respectively[20,21]. Constitutive dephosphorylation of LHCII in ΔSTN7 and PSII D1 and D2 subunits in ΔSTN8 *Arabidopsis* mutants leads to larger grana stacks, while constitutive phosphorylation of LHCII in ΔTAP38 and of PSII in ΔPBCP leads to smaller grana[21,22,23]. Dynamic changes in grana size and stacking have also been reported upon transitions in light intensity[24,25]. Dark, very low light and high light conditions favoured larger, more stacked grana whereas moderate light conditions (100-200 μmol photons m^{-2} s^{-1}) favoured smaller more numerous grana[24,25]. Similarly, under natural white light conditions maximal LHCII phosphorylation peaks under moderate light, with dephosphorylation occurring under dark, very low light and high light conditions[26]. PSII and LHCII phosphorylation are also known to affect the antenna sizes of PSI and PSII via a mechanism known as state transitions, which is provoked by changes in light colour rather than quantity in plants[27]. Yet the relationship between PSII/ LHCII phosphorylation, grana stacking and the LET/ CET balance in plants is not understood. Here we address this deficiency using a combination of biochemical, microscopic and spectroscopic methods to compare dark and growth light-adapted spinach plants.

RESULTS

Characterisation of light and dark thylakoids. Thylakoid membranes were prepared from 5 week old spinach plants grown at a moderate white light intensity of 200 μmol photons m^{-2} s^{-1}. Light adapted thylakoids were prepared from plants exposed for 1 hour to this growth light intensity, while dark-adapted plants were prepared after 1 hour of darkness. As expected the thylakoid composition of these two samples as judged by SDS-PAGE was identical (Fig. 1a), but their phosphorylation states revealed by Pro-Q diamond phosphoprotein staining were quite different (Fig. 1b). LHCII phosphorylation was increased and CP43 phosphorylation was decreased in the light compared to dark thylakoids, while phosphorylation of D1 and D2 was less dramatically affected (Fig. 1b), consistent with previous observations upon transition from dark to light[26,28]. Comparison of the low temperature (77K) fluorescence emission spectrum of the light and dark thylakoids revealed only a minor change in the PSI emission at 735 nm relative to the PSII emission bands at 685 and 695 nm (Fig. 1c), a clear contrast to the situation observed during state transitions provoked by changes in light colour, far-red to white or far-red to red/blue where a significant increase is seen[27,29,30,31]. Consistent with this we detected no significant change in the size of the PSI or PSII antenna by 77K fluorescence excitation spectroscopy, which would be observed as relative increases or decreases in excitation arising from the chlorophyll *b* regions of the spectrum at ~470 and ~650 nm (Figs. 1d and e). These findings were separately confirmed by PSI P700 absorption spectroscopy (Supplementary Fig. 1a) and fast PSII fluorescence induction (Supplementary Fig. 1b). We next investigated the distribution of LHCII between the grana and stromal lamellae thylakoids by fractionation of the membrane using the mild detergent digitonin. SDS-PAGE analysis of the grana and stromal lamellae fractions (Fig. 1a) indicated that the grana were relatively enriched in PSII and LHCII subunits compared to the thylakoids, while the stromal lamellae were more enriched in polypeptides belonging to PSI and ATP synthase. Western blotting confirmed that the cytb_6f complex was found in both the grana and stromal lamellae fractions with a slight preference for the latter (Fig. 1b), but no differences in the distribution were found between light and dark conditions. The SDS-PAGE (Fig. 1a) showed little change in the LHCII content of the grana or stromal lamellae upon shift from dark to light, further supported by the lack of change in the chlorophyll *b* contribution to their absorption spectra (Fig. 1f). Thus, the change in phosphorylation pattern associated with the transition from dark to light does not trigger any redistribution of LHCII between grana and stromal lamellae, unlike the state transition, where redistribution has been detected[32].

We next investigated the organisation of photosynthetic complexes within the grana and stromal lamellae domains by solubilising them and separating the components using BN-PAGE (Fig. 1g). The stromal lamellae were solubilised in 2% digitonin and the banding pattern revealed that the major constituents of these membranes were PSI-LHCI complexes, ATP synthase, PSII monomers, cytb_6f dimers and LHCII trimers (Fig. 1g and Supplementary Fig.1). The grana fraction is resistant to digitonin and so was solubilised in a blend of 0.5% *n*-hexadecyl β-D-maltoside/ 0.2% *n*-dodecyl α-D-maltoside. This causes a slightly increased migration for the complexes compared to digitonin (Fig. 1g). The composition of the grana was quite different as expected with major bands corresponding to PSII-LHCII supercomplexes, PSII dimers and monomers, cytb_6f dimers and LHCII trimers (Fig. 1g and Supplementary Figs. 1 c-f). A fraction of PSI-LHCI complexes was also observed in the grana sample, probably corresponding to a fraction of PSI more closely associated with the grana, that is often referred to as the 'margins' (Fig. 1g and Supplementary Fig.1)[25]. No differences in the amount of PSII-LHCII supercomplexes were observed in light-treated samples, but there was a strong increase in the amount of PSI-LHCI-LHCII supercomplexes in both the grana and stromal lamellae fractions, as well as a lowered level of oligomeric PSI-LHCI complexes (Fig. 1g and Supplementary Fig.1 c and d). Since the overall distribution of LHCII between the grana and stromal lamellae was unaltered, the LHCII required for formation of the PSI-LHCI-LHCII supercomplex most likely comes from the pre-existing pool of 'free' (L-type) LHCII trimers within these domains. Indeed, the stromal lamellae were recently reported to contain a significant amount of LHCII trimers in both the dark and light conditions[33].

Macromolecular organisation of grana thylakoids. We next investigated how the light to dark transition affected the organisation of PSII complexes, using atomic force microscopy (AFM) to image the grana membranes under aqueous buffer (Fig. 2a and b). As shown previously[34-36] the grana thylakoids are double membrane layers ~19.5 nm in height above the mica support (Fig. 2c (cross-sections marked in 2a and b). The sub-nanometer vertical resolution of the AFM is sufficient to identify protein complexes based on their high-resolution atomic structures. The faces of the grana thylakoids were covered with dimeric particles with heights of 4.1 ± 0.3 nm and 3.1 ± 0.3 nm above the surrounding membrane (Fig. 2d); these assignments are consistent with the lumenal protrusions of the PSII-LHCII supercomplexes[37] (h_1 in Fig. 2e) and cytb_6f[38] (h_2 in Fig. 2e) complexes respectively, and these assignments were recently confirmed by affinity-mapping AFM[35]. Analysis of the particle height distributions showed no significant difference between light and dark grana (Fig. 2d, Supplementary table 1), consistent with the unchanged levels of cytb_6f and PSII complexes (Fig. 1a and g). However, comparison of the nearest neighbour distributions of the particles on the grana membranes did reveal a significant difference (Fig. 2f, Supplementary table 1). The particles were more widely spaced in the light adapted membranes compared to the dark. Given the unchanged relative amounts of the C_2S_2 and C_2S_2M PSII-LHCII supercomplexes (Fig. 1g), this suggests that in the light the PSII-LHCII supercomplexes and cytb_6f become better mixed with the L-type LHCII trimers, which do not significantly protrude from the membrane surface[34-36].

Macromolecular organisation of stromal lamellae thylakoids. The protein organisation within the dark and light adapted stromal lamellae membranes was also investigated by AFM (Fig. 3a and b). The stromal lamellae thylakoids ranged in diameter from ~100-350 nm and were approximately 10 nm in height, with some larger topographic features 15.4 ± 2.0 nm in height (Fig. 3c). Mostly the stromal lamellae thylakoids are covered in particles that measured 3.2 ± 0.6 nm in height above the surrounding membrane (Fig. 3d), features that correspond well with the 3.2 nm height of the membrane extrinsic PsaC, D and E subunits on the stromal face of PSI-LHCI supercomplex from pea[39] (h_1 in Fig. 3e) and in AFM images of PSI from spinach[36], cyanobacteria[40] and observed in 2D crystals of detergent-purified PSI-LHCI supercomplexes[41]. Fig. 1b indicates that cytb_6f is present in our stromal lamellae thylakoids, but this proved more difficult to assign in our AFM images, probably owing to the small topographic features of cytb_6f on the stromal side of the membrane (h_2 in Fig. 3e). However, a discrepancy in the total height above the mica surface of the PSI-LHCI features (10.2 ± 0.6 nm, h_3 in Fig. 3e) to that predicted from the atomic structure[39] (8.2 nm h_4 in Fig. 3e) can be explained by the presence of cytb_6f protruding on the lumenal side of the stromal lamellae membranes and thus elevating PSI. If we assume the membrane is 4 nm in thickness[34-36] (h_5 in Fig. 3e), and the atomic structure of PSI-LHCI has a 1 nm protrusion on the lumenal side of the membrane (h_6 in Fig. 3e), the protein responsible for the additional elevation from the mica surface must possess lumenal protrusions

of 3.1 nm, which is consistent with cytb_6f (h_7 in Fig. 3e)[38]. Together heights h_1, h_5 and h_7 in Fig. 3e would account for the measured height of 10.2 ± 0.6 nm (h_3) above the mica surface, assigned as the PSI-LHCI supercomplex. Much larger protrusions that averaged 7.4 ± 1.4 nm in height are also present on the stromal lamellae thylakoids (Figs. 3a, b and d), which may be the CF_1 domain of the ATP synthase complex. The atomic structure of ATP synthase from *Bos taurus*[42] shows a 12.8 nm protrusion from the membrane surface (h_8 in Fig. 3e). On this basis, the observed protrusion seems too small to be the ATP synthase; however, AFM analysis of purified *Bos taurus* ATP synthase complexes incorporated into a lipid bilayer adsorbed onto mica showed a similar appearance and measured 7.3 ± 0.9 nm in height above the surrounding membrane (Supplementary Fig. 2a, b and c), consistent with the 7.4 nm features in the AFM topographs of stromal lamellae thylakoids. The purified ATP synthase and the 7.4 ± 1.4 nm protrusions seen in stromal membranes also showed similar diameters (Supplementary Fig. 2d). We therefore suggest that the 7.4 ± 1.4 nm features are the ATP synthase CF_1 domain (h_9 in Fig. 3e), which is smaller than expected due to reversible deformation upon contact with the downward motion of the AFM probe. The distributions in the particle heights for stromal lamellae membranes from the light or dark treated thylakoids were not significantly different (Fig. 3d, Supplementary table 2), consistent with their unchanged composition (Fig. 1a and g). A significant difference was found in the nearest neighbour distributions in the light and dark stromal lamellae thylakoids (Fig. 3f), suggesting that PSI particles adopt a tighter packing in the dark. A portion of the PSI in the thylakoid fractionates with the grana membranes (Fig. 1a and g). AFM images showed that this PSI population arises from grana membranes that are still contiguous with adjoining stromal lamellae membranes (Supplementary Fig. 3a). Comparison of the nearest neighbour distance between these regions and the stromal lamellae fraction suggests they have a similar organisation (Supplementary Fig. 3b).

Dimeric arrangement of PSI-LHCI complexes. We noticed a tendency for the PSI particles in our AFM images to form dimeric pairs in many of the images (Fig. 4a), with a consistent spacing of 12.4 ± 1.0 nm (Fig. 4b). In contrast to the dimeric, trimeric and tetrameric structures of PSI in cyanobacteria[43], plant PSI purifies and crystallises as a monomer[39]. Using the atomic structure of monomeric PSI-LHCI we modelled possible arrangements of the dimers in Fig. 4c-e and show the intercomplex distance measured from one protruding PsaC subunit to another. The dimers we observe in the membrane are most consistent with a model in which PSI-LHCI supercomplexes are arranged with their PsaB to PsaH subunits facing one another (Fig. 4c). Dimers of PSI-LHCI supercomplexes with this spacing are consistent with a single-particle electron microscopy (EM) structure recently isolated in low abundance from the stromal lamellae using the detergent digitonin[44]. Our results indicate that this dimeric PSI supercomplex is relatively common in the intact membrane and it can even form ordered rows (Fig. 4a). Comparison of the number of PSI-LHCI dimers in dark and light adapted membranes revealed a significant decrease in the latter (Supplementary table 2), consistent with this the amount of oligomeric PSI-LHCI recovered in the BN-PAGE gels of stromal lamellae also decreases in the light adapted state (Fig. 1g).

Thylakoid stacking changes. We investigated the response of thylakoid stacking to the dark to light transition using both structured illumination microscopy (SIM) and thin-section transmission EM. SIM excites the sample with a series of precisely known illumination patterns, allowing reconstruction of a high-resolution optical image, with 2-fold increase in resolution, in each lateral direction, compared to confocal fluorescence microscopy and for three-dimensional volumetric imaging there is an overall 8-fold improvement; typical resolutions are ~120 nm (xy) and ~320 nm (z)[45]. SIM allows the 3D imaging of intact chloroplasts without the use of fixatives or dehydration as used in thin section EM. The samples were excited with 640 nm light and the chlorophyll emission collected between 660 and 700 nm. The images shown in Fig. 5a are consecutive slices 125 nm in depth, through intact chloroplasts from light and dark-adapted plants. The bright fluorescent regions are the PSII dominated grana membranes, while the less fluorescent spindly interconnecting regions are the stromal lamellae. Analysis of the grana diameter using the FWHM of the signal from each granum revealed a significant decrease in light compared to dark adapted samples (Fig. 5b, Supplementary table 3), while the number of grana per chloroplast increased (Fig. 5c, Supplementary table 3). We confirmed these changes using thin-section EM on leaves (Fig. 5d and e); in light versus dark chloroplasts the layers per granum (Fig. 5f) and grana diameter decreased (Supplementary Fig. 4a) and the number of grana per chloroplast increased (Supplementary Fig. 4b). These changes

significantly increase the number grana end membranes, i.e. the membranes at the very top and bottom of the grana stack, which have a similar or identical composition to the stromal lamellae but are in close contact with grana membranes across the lumenal gap. Moreover, the relative area of contact between grana and stromal lamellae membranes is increased by the smaller granal size. It was previously reported that a dark to light transition results in the expansion of the thylakoid lumen[46], however under our conditions this was not the case (Supplementary Fig. 4c to f), which may reflect the lower light intensity used in this study. We also checked that phosphorylation was directly responsible for the changes in thylakoid architecture by infiltrating light adapted leaves in a buffer with and without NaF to inhibit dephosphorylation, before dark adapting them for a further hour, giving two samples we term Light/Dark-NaF (Fig. 5g) and Light/Dark+NaF (Fig. 5h). The Light/Dark+NaF leaves showed features consistent with those of light adapted leaves with smaller grana compared to the Light/Dark–NaF leaves (Fig. 5i), suggesting that the stacking changes are due to phosphorylation.

Effects on electron transfer and photoprotection. The net result of the stacking changes we observe is a reduction the average distance from a complex localised within the grana to one localised within the stromal lamellae. This change has the potential to affect diffusion limited electron transfer processes mediated by the PQ and PC carriers within the thylakoid membrane[47]. Indeed, PC diffusion is further assisted by the increased number of grana end membranes, which directly face grana membranes across the lumen. Therefore, we sought to model how these changes in thylakoid architecture might affect the diffusion of PQ and PC through the membrane bilayer and in the lumen respectively. We used our AFM data to construct a 3-D model of the lumenal space, which is crowded by the protruding parts of cytb_6f and PSII, and performed a Monte Carlo simulation of PC diffusion within this space (Fig 6a). The simulation suggests a 25% decrease in the time taken for PC to diffuse from cytb_6f in the grana to PSI in the stromal lamellae in light compared to dark adapted thylakoids (Fig. 6b), independent of the total interface size used between the domains (Supplementary Fig. 5a) and considering the increase in axial short-range diffusion to grana end membranes in the light (Supplementary Fig. 5b and see Methods). Monte Carlo simulations, again based on our AFM data, also predicted 13.4% faster PQ diffusion through the membrane from PSII in the grana to cytb_6f in the stromal lamellae in the light adapted thylakoids (Fig. 6c), again independent of the total interface size used (Supplementary Fig. 5c). Consistent with these predictions of faster diffusion of electron carriers we found that PSI reduction following a 250 ms saturating light pulse was significantly faster in the light adapted leaves, suggesting enhanced electron flow to PSI (Fig. 6d). PSI reduction was faster in the light adapted leaves both in the presence of methyl viologen (MV) as a PSI electron acceptor, which removes any differences arising CET contribution and/or Calvin-Benson cycle activation between the samples (Fig. 6d), as well as in its absence (Supplementary Fig. 5d). The difference was also maintained in Light/Dark+NaF leaves compared to Light/Dark-NaF leaves in the presence of MV (Fig. 6e). These results suggest that the smaller more numerous stacks in light adapted and Light/Dark+NaF leaves speed up the electron flow to PSI, consistent with the simulation.

PSI reduction was previously shown to be enhanced in dark compared to light adapted leaves following far-red illumination, conditions that preferentially excite PSI[4,48]. The enhanced reduction of PSI under far-red was attributed to an increased contribution of CET[4,48]. Consistent with these findings we observed faster PSI reduction in the dark compared to light adapted leaves following far-red illumination (Fig. 6f). However, we also found that PSI reduction following far-red light was significantly faster in the Light/Dark-NaF compared to Light/Dark+NaF leaves (Fig. 6g), suggesting that the larger grana stacks in the dephosphorylated state may somehow enhance CET. To confirm that a difference in PSI reduction under far-red illumination reflects real changes in CET capacity we monitored transient NPQ. Transient induction of NPQ is seen in dark adapted leaves exposed to the growth light due a build-up of ΔpH associated with enhanced CET during photosynthetic induction, whereas in light adapted leaves it is absent since the Calvin-Benson cycle is already active (Fig. 6h)[8,9]. The NPQ transient was found to be suppressed in the Light/Dark+NaF compared to the Light/Dark-NaF leaves (Fig. 6h). The lower NPQ meant that PSII photochemical quenching (qP) is suppressed in the Light/Dark+NaF leaves in the light due to the higher excitation pressure and recovered less in the subsequent dark period, indicative of photoinhibitory damage (Fig. 6i)[49]. Thus, the smaller more numerous grana stacks in the Light/Dark+NaF leaves are associated with a lower efficiency of CET upon dark to light transition and thus ΔpH and protective NPQ are suppressed.

Grana stacking in plants has been suggested to create separate pools of PQ in the grana and stromal

lamellae isolated by diffusion limitation[15,16]. Indeed, it was previously shown that PSII is in fast redox contact with only around 60-70% of the PQ pool, which is reduced with a half time of ~25 ms, whereas the remaining 20-30% is reduced with a half-time of ~6 s[15]. The fast and slow PQ pools were attributed to the grana and stromal lamellae respectively. If the two pools were better equilibrated in light adapted thylakoids due to faster granal to stromal lamellae PQ diffusion, as suggested by our Monte Carlo simulation, then the reduction time should be increased. Using fast PSII fluorescence induction in the presence of 2,5-dibromo-6-isopropyl-3-methyl-1,4-benzoquinone (DBMIB), to block PQH_2 oxidation by cytb_6f, allowed us to follow the rate of PQ reduction in dark and light adapted leaves. The PQ pool is more rapidly reduced in dark adapted compared to light adapted leaves, despite the identical antenna sizes (Fig. 6j). This result could suggest that a larger pool of PQ is available for PSII to reduce in the light adapted leaves. A similar decrease in the rate of PQ reduction was found in the Light/Dark+NaF compared to the Light/Dark-NaF leaves, suggesting the changes are due to the alterations in thylakoid stacking (Fig. 6k).

DISCUSSION

The results presented lend further support to recent work[30,50] showing that changes in PSII and LHCII phosphorylation provoked by varying white light quantity do not significantly alter the relative antenna sizes of PSI and PSI in plants. This is a clear contrast to the changes in phosphorylation provoked by light colour, where significant changes in PSI and PSII are detected[18-21,30-32]. Unlike in state transitions where far-red light leads to complete dephosphorylation of both PSII and LHCII and low intensity red or blue light leads to their hyperphosphorylation[30], here CP43 was more phosphorylated in the dark and LHCII less so, while D1 and D2 phosphorylation changed little. Yet, both state transitions[29,31,51] and the dark to light transition (Fig. 1g) led to a large increase in the amount of the PSI-LHCI-LHCII supercomplex detected. How can these results be reconciled? Since in this study we found no evidence for the movement of LHCII from the grana to stromal lamellae, it suggests the LHCII incorporated into the PSI-LHCI-LHCII supercomplex is already present in the stromal lamellae. Indeed, as noted previously dark-adapted stromal lamellae already contain a significant pool of L-type LHCII trimers[33]. Recent work has shown that PSI binds significantly more LHCII *in vivo* than can be accounted for in the PSI-LHCI-LHCII supercomplex[29,52,53]. The results here therefore support the idea that the L-type LHCII forms a 'lake' that serves both PSII and PSI[29]. Thus, it seems likely that the LHCII in the stromal lamellae is energetically connected to PSI irrespective of whether it can be recovered still attached to PSI by digitonin solublisation[29,33]. In line with this, a growth light (120 μmol photons m^{-2} s^{-1}) to high light (1000 μmol photons m^{-2} s^{-1}) transition in *Arabidopsis* causes disappearance of the PSI-LHCI-LHCII supercomplex, but no decrease in PSI antenna size[30]. We suggest that the appearance of the PSI-LHCI-LHCII supercomplex may reflect phosphorylation driven reorganisation of the stromal lamellae membrane that we observe by AFM. The light-adapted state showed fewer PSI-LHCI dimers and a greater separation between PSI-LHCI complexes. Similarly, our AFM showed that the PSII nearest neighbour distance in the grana was significantly increased when LHCII was phosphorylated in the light adapted state. These results suggest that the L-type LHCII becomes better mixed with PSI and PSII in the light adapted state, whereas its dephosphorylation in the dark drives its self-association and clustering, reducing its dispersal amongst PSI and PSII. These changes are achieved without significantly altering the PSII and PSI antenna sizes as the system is so packed (70-80% protein density) that energetic connectivity is maintained irrespective of the exact arrangement of the L-type LHCII[54].

As well as causing changes in the organisation of PSI and PSII complexes within the stromal lamellae, the dark to light transition also caused changes in thylakoid stacking. The grana diameter and number of membrane layers per grana are decreased in the light but the number of grana per chloroplast is increased. Therefore, in light adapted chloroplasts there is a movement towards smaller more numerous grana. By infiltrating light-adapted leaves with NaF prior to dark adaptation we could show that the changes in grana stacking depend on phosphorylation. This observation is in line with the differences in thylakoid stacking observed in *Arabidopsis* mutants lacking the STN7 or STN8 kinases and PBCP or TAP38 phosphatases[21-23]. The organisation of the grana in the dark more closely resembles that seen under high light conditions[55], where LHCII is also dephosphorylated[26,30]. Both dark and high light conditions lead to fewer but larger grana compared to moderate light[24]. As well as promoting increased lateral LHCII-LHCII interactions, dephosphorylation also reduces the net charge on the complex[17] increasing the attraction between the stromal faces of LHCII in separate grana layers, enhancing grana stacking. Indeed, in plants grown on lincomycin, which largely lack PSII, huge LHCII-only grana are formed suggesting stacking is

enhanced by LHCII clustering[56].

The net result of the changes in stacking modulated by LHCII phosphorylation level is that it reduces the average distance from a complex localised within the grana to one localised within the stromal lamellae. Our Monte Carlo simulations based on the AFM and EM/SIM data predicted that these changes in grana stacking should affect the diffusion time for both PQ and PC. These predictions were born out by the faster PSI reduction kinetics in light compared to dark adapted leaves, indicating the efficiency of electron flow to PSI is enhanced. In contrast, when we probed PSI reduction following far-red illumination the opposite picture emerged. Dark-adapted leaves showed faster reduction under these conditions than light-adapted leaves, consistent with enhanced CET[4]. The lower propensity for CET in light-adapted material reflects the activation of the Calvin-Benson cycle and thus diversion of electrons to LET, reducing the number of cycled electrons and so slowing PSI reduction following far-red illumination[4,48]. These differences in CET activity could simply represent differences in the redox state of the stroma in dark compared to light adapted leaves, rather than the alterations in thylakoid structure. We tried to distinguish the contribution of these two factors using the Light/Dark+NaF and Light/Dark-NaF treated leaves, the former retaining small grana in the dark. The results showed that following a saturating light pulse PSI reduction was still significantly faster in the Light/Dark+NaF leaves, supporting the conclusion that electron flow to PSI is enhanced by the phosphorylation-driven reduction in grana size. This conclusion is consistent with the increased efficiency of LET in the ΔTAP38 mutant[20], which has smaller grana and reduced LET efficiency in the ΔCURT mutant of *Arabidopsis*[23], which has much larger grana. In contrast, following far-red illumination the reduction of PSI was faster in the Light/Dark-NaF leaves, supporting the view that the dephosphorylation-driven increase in grana size in the dark enhances the efficiency of CET. This conclusion was supported by the increased transient NPQ generated in the Light/Dark-NaF leaves, that better protected PSII from photoinhibition.

Based on our findings we hypothesise that the significance of the structural changes associated with white light driven LHCII phosphorylation is in controlling the balance between LET and CET, rather than modifying the antenna sizes of the photosystems. In moderate light, LET predominates and LHCII phosphorylation ensures that the grana size is small and the relative area of contact with the stromal lamellae is large (Fig. 7a). Under these conditions, PQ and PC can flow more freely from the grana to stromal lamellae because of the decreased diffusion time associated with the shorter distances involved (Fig. 7a). The net result is a more efficient LET, since cytb_6f in both the grana and stromal lamellae is involved in oxidising PSII-derived PQH_2. In the first few minutes following illumination of dark adapted plants there is a need for enhanced CET since the PSI acceptor side is limited by the slow activation of the Calvin-Benson Cycle. CET induced build-up of ΔpH protects PSII through NPQ and avoids over-reduction of PSI via downregulation of the cytb_6f complex[6]. For efficient activation of CET there must be a relatively oxidised pool of PQ ready to accept electrons from either the NDH or PGRL1/PGR5 CET pathways. The increased grana stacking in the dark brought about by dephosphorylation of LHCII ensures this by enhancing the segregation of the granal and stromal pools of PQ associated with the cytb_6f complexes in each domain, ensuring PSII can only reduce the granal pool on fast timescales (Fig. 7b). It is noteworthy that very low light and high light conditions that also provoke dephosphorylation of LHCII and increased grana stacking[24] are also suggested to be associated with higher CET activities[12,57,58]. In conclusion our results support the view that the domain structure of the plant thylakoid membrane ensures separate pools of PQ exist[15,16], which are vital to limit competition between the LET and CET pathways under conditions where significant CET is needed. Further, the dynamics of grana stacking modulated by LHCII phosphorylation likely controls degree of PQ segregation and so the balance between LET and CET.

METHODS

Plant Growth. Spinach (*Spinecea oleracea*) plants were grown for 5 weeks in a Conviron plant growth room with a 12 hour photoperiod at a light intensity of 200 μmol photons m^{-2} sec^{-1} and a day/night temperatures of 22/18°C, respectively.

Preparation of membranes. Thylakoid membranes were prepared from spinach leaves either dark adapted for 1 hour or adapted to the growth light conditions (200 μmol photons m^{-2} sec-1) for 1 hour according to Albertsson et al[59], with the addition that 10 mM NaF was included in all buffers. Grana membranes were prepared by solubilising thylakoid membranes suspended in 5 mM $MgCl_2$/ 10 mM NaF/ 10 mM HEPES-NaOH pH 7.4 at a final concentration of 0.5 mg/ml chlorophyll with 2% (w/v) digitonin for 1 hour on ice.

Unsolubilised thylakoids were removed by centrifugation at 10 000 g for 30 minutes and the supernatant was then spun at 40 000 g to pellet the grana membranes. The pellet was then resuspended in 5 mM $MgCl_2$/ 10 mM NaF/ 10 mM HEPES-NaOH pH 7.4 and centrifuged on a 10 – 45 % (w/w) continuous sucrose density gradient containing 10 mM NaF/ 10 mM HEPES-NaOH pH 7.4 / 0.1% digitonin using a Beckman SW41 rotor at 200 000 g for 2 hours. Stromal lamellae membranes were prepared by solubilising thylakoid membranes suspended in 5 mM $MgCl_2$/ 10 mM NaF/ 10 mM HEPES-NaOH pH 7.4 at a final concentration of 0.5 mg/ml chlorophyll with 0.75% (w/v) digitonin for 1 hour on ice. Unsolubilised thylakoids and grana membranes were removed by centrifugation at 40 000 g for 30 minutes and the supernatant was then centrifuged on a 10 – 45 % (w/w) continuous sucrose density gradient containing 10 mM NaF/ 10 mM HEPES-NaOH pH 7.4 / 0.1% digitonin using a Beckman SW41 rotor at 200 000 g for 2 hours.

SDS-PAGE. Membranes (5μg of chlorophyll) were solublised in Laemmli buffer and separated by SDS-PAGE and stained with Coomassie according to Benson et al.,[29]. Diamond Pro-Q Phospho staining (Life technologies) and Immunoblotting using an anti-PetC antibody (Agrisera) were performed as previously described by Mekala et al.,[30].

Blue-Native PAGE. Grana membranes were solubilized with 0.5% (w/v) *n*-hexadecyl β-D-maltoside/ 0.2% (w/v) *n*-dodecyl α-D-maltoside and stromal lamellae by 2% (w/v) digitonin both for 10 minutes at room temperature. The samples were then subjected to BN-PAGE and subsequently separated by 2D-denaturing PAGE as described by Mekala et al.,[30]

Low temperature fluorescence spectroscopy. 77K fluorescence spectroscopy was carried out as described in Benson et al, [29].

PSI absorption measurements. P700 absorption was measured in the dual-wavelength mode (830 nm-875 nm) of the Dual PAM 100 (Walz). $P700^+$ oxidation kinetics (Supplementary Fig. 1a) were measured on light or dark adapted leaves vacuum infiltrated with 30 μM 3-(3,4-dichlorophenyl)-1,1-dimethylurea (DCMU) / 1 mM MV/ 50 mM NaF/ 10 mM HEPES-NaOH pH 7.4/ 150 mM sorbitol. Under these donor-limited conditions the rate of photo-oxidation of P700 is directly proportional to the PSI antenna size[60]. The light intensity was 12 μmol photons m^{-2} s^{-1}. P700 reduction was measured on the same device following a 250 ms light flash with an intensity of 2000 μmol photons m^{-2} s^{-1} using light or dark adapted leaves vacuum infiltrated with 50 mM NaF/ 10 mM HEPES-NaOH pH 7.4/ 150 mM sorbitol with (Fig. 6d) or without 1 mM MV (Supplementary Fig. 5d). P700 reduction was also monitored following 20 s of far-red light (720 nm) with an intensity of 100 μmol photons m^{-2} s^{-1} using light or dark adapted leaves vacuum infiltrated with 50 mM NaF/ 10 mM HEPES-NaOH pH 7.4/ 150 mM sorbitol (Fig. 6f).

PSII fluorescence induction measurements. Chlorophyll fluorescence induction for determination of PSII antenna size (Supplementary Fig. 1b) was measured with a Dual PAM 100 (Walz) on light or dark adapted leaves infiltrated with 30 μM DCMU/ 50 mM NaF/ 10 mM HEPES-NaOH pH 7.4/ 150 mM sorbitol using a light intensity of 12 μmol photons m^{-2} s^{-1}. The fluorescence rise time from Fo to Fm is inversely proportional to the antenna/RCII chlorophyll ratio (PSII antenna size) quantified as described previously[54]. The reduction of PQ (Fig. 6j) was assessed using chlorophyll fluorescence induction in light and dark adapted leaves infiltrated with 20 μM nigericin/ 80 μM DBIMB/ 50 mM NaF/ 10 mM HEPES-NaOH pH 7.4/ 150 mM sorbitol either by continuous illumination using a light intensity of 6 μmol photons m^{-2} s^{-1}, or by giving leaves a 500 ms 2000 μmol photons m^{-2} s^{-1} saturating pulse followed by a variable dark period (5-30s) prior to 1500 ms fluorescence induction curve induced by 6 μmol photons m^{-2} s^{-1} illumination[15]. For NPQ measurements leaves were subjected to 5 minutes illumination with 200 μmol photons m^{-2} s^{-1} light and then allowed to recover in the dark for 3 minutes. The measuring beam intensity for all measurements was 6 μmol photons m^{-2} s^{-1}.

Treatment for Light/Dark-NaF and Light/Dark+NaF leaves. PSII fluorescence and PSI absorption experiments identical to those described above were carried out for leaves light adapted for 1 hour at 200 μmol photons m^{-2} sec^{-1}, then vacuum infiltrated with 10 mM HEPES-NaOH pH 7.4/ 150 mM sorbitol either

with 50 mM NaF (Light/ Dark+NaF) or without (Light/Dark-NaF), and then dark adapted for a further 1 hour prior to the measurements.

AFM. Grana and stromal lamellae membrane fractions obtained from the sucrose gradients were diluted 10-fold and adsorbed to freshly-cleaved mica for 15 minutes in 10 mM HEPES (pH 7.4), 5 mM $MgCl_2$ and 125 mM KCl and imaged in the same buffer. Imaging was performed using PeakForce quantitative nanomechanical mapping mode on a Bruker Multimode VIII AFM. Bruker SNL-10 C triangular probes (nominal spring constant: 0.24 N/m) were used. During imaging the PeakForce setpoint was set at 0.03 – 0.04 V in order to prevent damage to the probe and sample. The PeakForce amplitude was set at 15 nm.

Incorporation of *Bos Taurus* ATP synthase into DOPC liposomes. *Bos Taurus* ATP synthase was purified according to ref 42. 1 mg/ml DOPC was prepared in 20 mM MOPS (pH 7.8), 20 mM NaCl and was extruded 40 times using a 200 nm filter. ATP synthase was added at a ratio of 50 µl / 200 µl liposomes and was incorporated into the liposomes in the presence 0.004 % βDDM for 1 hour on ice.

Data analysis and visualisation. All graphs were created using Graphpad Prism 7. PSII fluorescence induction and PSI absorption curves show mean ± standard error at each time point. All box plots contain error bars which display mean ± standard deviation. AFM images were produced using Bruker's NanoScope Analysis 1.5 software. Membrane cross section data were extracted using NanoScope Analysis 1.5 and displayed using Graphpad Prism 7. Particle coordinates were extracted from AFM images using the read value under mouse cursor function of Gwyddion 2.42. Heights of the particles, as measured from the membrane and the mica, were calculated by subtracting the heights of the membrane and mica respectively from the raw height measurement of the particle. In all images, a plane was fitted through 3 points on the mica surface and subtracted to remove any tilt and the minimum z value was set to zero before measurements were taken. Nearest neighbour distances between particles refer to lateral distance $\sqrt{(\Delta x^2+\Delta y^2)}$ and were calculated using a custom Python script. Histograms along with Gaussian least-square fit curves for both height and nearest neighbour analyses were produced using Graphpad prism 7. PDB structures were displayed using PyMOL software.

Modelling and Monte Carlo simulation. Random walk simulations were carried out on a 2-Dimensional or 3-Dimensional (for PQ and PC simulations respectively) square lattice with 1 nm spacing, for interface sizes ranging from 10-90 % grana perimeter. Diffusion coefficients for PQH_2 and PC of 3.5 x 10^{-7} cm^2 s^{-1} and 0.9 x 10^{-8} cm^2s^{-1} were used respectively[61,62]. The grana were composed of two layers separated by 10 nm (Fig. 6a) and had radii of 190 nm (dark) and 170 nm (light) (as per Fig. 5b). Each contained particles of radius 6.7 nm at a density of 1.14 × 10^{-3} nm^{-2} (determined from AFM data). We assumed equal numbers of C_2S_2 and $C_2S_2M_2$ PSII-LHCII supercomplexes (Fig. 1g) and an additional 2.5 LHCII trimers per each PSII RC[63]. *Cytb$_6$f* particles were added to the grana and stromal lamellae at a ratio of 30/70 (Fig. 1b) and at a density of 60 % of the number of PSI[64]. The stromal lamellae consisted of two layers, also separated by 10 nm, each a 50 nm concentric circle of the grana (in order to produce a PSI/PSII of 1.13[63]), containing particles of radius 5 nm at a density of 2.45 × 10^{-3} nm^{-2} (determined from AFM data). The particle radii were determined from the smallest observed nearest neighbour values in the AFM data. The grana particles (taking into account the approximation of 1 nm for the radius of PC) protruded into the lumenal space effectively by 5 nm as cylinders of radius 6.7 nm. For each random walk simulation, a PQH_2 was spawned at a random PSII site and allowed to move by Brownian motion until a *cytb$_6$f* was reached. For plastocyanin, the particle was spawned at a random grana particle and a random walk was generated until the plastocyanin particle came within the radius of a PSI particle in the stromal lamellae. The number of time steps was recorded and converted into time using the equation:

$$\langle X^2 \rangle = 2dD\Delta t$$

where X is the grid spacing of 1 nm as previously described and d is the dimensionality.
For end-membrane PC transport, one of the grana layers was replaced with a layer of stromal lamellae of the same size.
To calculate diffusive times for general PC transport incorporating end-membranes, times for PC diffusion were sampled from the distributions of grana to stromal lamellae PC transport and grana to end membrane

PC transport with probabilities of $\frac{2N-2}{2N}$ and $\frac{2}{2N}$ respectively, where N was the average number of lumenal spaces per grana stack as measured using thin-section EM.

Structured illumination acquisition and analysis. Intact chloroplasts prepared as in Johnson et al.,[55] were sealed in Vectashield (Vector Laboratories) and imaged on a DeltaVision OMX V4 microscope (GE Healthcare) equipped with the Blaze-3D SIM module and 60x 1.42 oil planapochromat lens. Chloroplast fluorescence was excited with a 642 nm laser and the emission was collected through a 683/40 nm bandpass filter. The structured illumination pattern was projected onto the sample in a series of five phases for each of three angles leading to a total of 15 images per axial slice. The 3D image was acquired via sectioning with a 2D slice separation of 125 nm. The final super-resolution image was reconstructed with the SoftWoRx OMX 6.0 software (GE Healthcare). Grana widths were measured as the full-width half-maximum of a line profile across the granal-midpoint in images that had been thresholded and 16-bit converted with the SIMcheck plugin for ImageJ.

Electron microscopy. Spinach leaves were fixed by infiltrating with 3% glutaldehyde/0.1M sodium cacodylate buffer overnight, washed in buffer and post fixed 2% osmium tetroxide, washed briefly in water and dehydrated through a graded series of ethanol treatments, cleared in epoxypropane (EPP) and infiltrated in a 50/50 araldite resin:EPP mixture overnight on a rotor. This mixture was replaced two changes, over 8 hours, with fresh araldite resin mixture before being embedded and curing in a 60°C oven for 48-72 hours. Ultrathin sections, approximately 85 nm thick, were cut on a Leica UC 6 ultramicrotome onto 200 mesh copper grids, stained for 30 mins with saturated aqueous Uranyl Acetate followed by Reynold's Lead Citrate for 5 mins. Sections were examined using a FEI Tecnai Transmission Electron Microscope at an accelerating voltage of 80Kv. Electron micrographs were recorded using a Gatan Orius 1000 digital camera and Digital Micrograph software.

Data availability. The data that support the findings of this study are available from the corresponding author upon request.

References

1. Horton, P. Interactions between electron transfer and carbon assimilation. In: Barber J and Baker NR (eds) Photosynthetic Mechanisms and the Environment, pp 135- 187. Elsevier, Amsterdam, New York (1985)
2. Robinson, S. P. & Walker, D. A. The control of 3-phosphoglycerate reduction in isolated chloroplasts by the concentrations of ATP, ADP and 3-phosphoglycerate. *Biochim. Biophys. Acta* **545**, 528-536 (1979).
3. Slovacek, R.E., Crowther, D. & Hind, G. Relative activities of linear and cyclic electron flows during chloroplast CO_2 fixation. *Biochim. Biophys. Acta* **592**, 495-505 (1980).
4. Joliot, P. & Joliot, A. Quantification of cyclic and linear flows in plants. *Proc. Nat. Acad. Sci. USA* ***102,*** 4913-4918 (2005).
5. Yamori, W. & Shikanai, T. Physiological functions of cyclic electron transport around photosystem I in sustaining photosynthesis and plant growth. *Annu. Rev. Plant Biol.* **67**, 81-106 (2016).
6. Johnson, G. N. Physiology of PSI cyclic electron transport in higher plants *Biochim. Biophys. Acta* **1807**, 384-389 (2011).
7. Soursa, M. *et al*. Proton gradient regulation 5 is essential for proper acclimation of *Arabidopsis* photosystem I to naturally and artificially fluctuating light conditions. *Plant Cell* **24**, 2394-2948 (2012).
8. Munekage, Y. *et al*. Cyclic electron flow around photosystem I is essential for photosynthesis. *Nature* **429**, 579-582 (2004).
9. Herte, A. P. *et al.* PGRL1 is the elusive ferredoxin–plastoquinone reductase in photosynthetic cyclic electron flow. *Mol. Cell* **49**, 511-523 (2013).
10. Avenson, T. J., Cruz, J. A, Kanazawa, A. & Kramer, D. M. Regulating the proton budget of plant photosynthesis. *Proc. Nat. Acad. Sci. USA* **102**, 9709-9713 (2005).

11. Strand, D., Fisher, N. & Kramer, D. M. The higher plant plastid NAD(P)H dehydrogenase-like complex (NDH) is a high efficiency proton pump that increases ATP production by cyclic electron flow. *J. Biol. Chem*. **292,** 11850-11860 (2017).

12. Yamori, W., Shikanai, T. & Makino, A. Photosystem I cyclic electron ow via chloroplast NADH dehydrogenase-like complex performs a physiological role for photosynthesis at low light**.** *Sci. Rep.* **5**, 13908 (2015).

13. Iwai, M. *et al*. Isolation of the elusive supercomplex that drives cyclic electron flow in photosynthesis. *Nature* **464**, 1210-1213 (2010).

14. Takahashi, H., Clowez, S., Wollman, F. A., Vallon, O. & Rappaport, F. Cyclic electron flow is redox-controlled but independent of state transition. *Nature Comm*. **4**, 1954 (2013)

15. Joliot, P., Lavergne, J. & Beal, D. Plastoquinone compartmentation in chloroplasts. I. Evidence for domains with different rates of photo-reduction. *Biochim. Biophys. Acta* **1101**, 1-12 (1992).

16. Dumas, L., Chazaux, M., Peltier, G., Johnson, X. & Alric, J. Cytochrome b6f function and localization, phosphorylation state of thylakoid membrane proteins and consequences on cyclic electron flow. *Photosyn. Res*. **29**, 307–320 (2016).

17. Puthiyaveeti, S., van Oort, B. & Kirchhoff, H. Surface charge dynamics in photosynthetic membranes and the structural consequences. *Nature Plants* **3**, 17020 (2017).

18. Bellafiore, S., Barneche, F., Peltier, G. & Rochaix, J. D. State transitions and light adaptation require chloroplast thylakoid protein kinase STN7. *Nature* **433**, 892–895 (2005).

19. Bonardi, V. *et al.* Photosystem II core phosphorylation and photosynthetic acclimation require two different protein kinases. *Nature* **437**, 1179–1182 (2005)

20. Pribil, M., Pesaresi, P., Hertle, A., Barbato, R. & Leister, D. Role of plastid protein phosphatase TAP38 in LHCII dephosphorylation and thylakoid electron flow. PLoS Biol. **8**, e1000288 (2010).

21. Samol, I. *et al*. Identification of a Photosystem II Phosphatase Involved in Light Acclimation in *Arabidopsis*. *Plant Cell* **24**, 2596–2609 (2012).

22. Fristedt, R. *et al.* Phosphorylation of photosystem II controls functional macroscopic folding of photosynthetic membranes in Arabidopsis. *Plant Cell* **21,** 3950–3964 (2009).

23. Armbruster, U. *et al. Arabidopsis* CURVATURE THYLAKOID1 proteins modify thylakoid architecture by inducing membrane curvature. *Plant Cell* **25,** 2661–2678 (2013)

24. Rozak, P. R., Seiser, R. M., Wacholtz, W. F. & Wise, R. R. Rapid, reversible alterations in spinach thylakoid appression upon changes in light intensity. *Plant Cell Environ.* **25,** 421–429 (2002).

25. Anderson, J. M., Horton, P., Kim, E.-H. & Chow, W. S. Towards elucidation of dynamic structural changes of plant thylakoid architecture. *Phil. Trans. Roy. Soc. London* **367,** 3515–3524 (2012).

26. Rintamaki, E. *et al*. Phosphorylation of Light-harvesting Complex II and Photosystem II Core Proteins Shows Different Irradiance-dependent Regulation *in Vivo*. *J. Biol. Chem.* **272**, 30476-30482 (1997).

27. Ruban, A. V. & Johnson, M. P. Dynamics of higher plant photosystem cross- section associated with state transitions. *Photosynth. Res*. **99**, 173–183 (2009).

28. Fristedt, R., Granath, P. & Vener, A. V. A Protein Phosphorylation Threshold for Functional Stacking of Plant Photosynthetic Membranes. *PLoS One* **5**, e10963 (2010).

29. Benson, S. L. *et al.* An intact light harvesting complex I antenna system is required for complete state transitions in Arabidopsis. *Nature Plants* **1**, 15176 (2015).

30. Mekala, N. R., Soursa, M., Rantala, M. Aro, E.M. & Tikkanen, M. Plants Actively Avoid State Transitions upon Changes in Light Intensity: Role of Light-Harvesting Complex II Protein Dephosphorylation in High Light. *Plant Phys.* **168**, 721-734 (2015).

31. Wientjes, E., van Amerongen, H. & Croce, R. LHCII is an antenna of both photosystems after long-term acclimation. *Biochim. Biophys. Acta* **1827**, 420-426 (2013).

32. Kyle, D. J., Staehelin, L. A. & Arntzen, C. J. Lateral mobility of the light- harvesting complex in chloroplast membranes controls excitation energy distribution in higher plants. *Arch. Biochem. Biophys*. **222,** 527–541 (1983).

33. Grieco, M., Suorsa, M., Jajoo, A., Tikkanen, M. & Aro, E. M. Light-harvesting II antenna trimers connect energetically the entire photosynthetic machinery - including both photosystems II and I. *Biochim. Biophys. Acta* **1847**, 607–619 (2015).

34. Sznee, K. *et al.* Jumping mode atomic force microscopy on grana membranes from spinach. *J. Biol. Chem.* **286,** 39164–39171 (2011).

35. Johnson, M. P., Vasilev, C., Olsen, J. D. & Hunter, C. N. Nanodomains of cytochrome *b6f* and photosystem II complexes in spinach grana thylakoid membranes. *Plant Cell* **26,** 3051–3061 (2014).

36. Phuthong, W. *et al.* e use of contact mode atomic force microscopy in aqueous medium for structural analysis of spinach photosynthetic complexes. *Plant Physiol.* **169,** 1318-1332 (2015).

37. Su, X. *et al*. Structure and assembly mechanism of plant C2S2M2-type PSII-LHCII supercomplex. *Science* **357**, 815-820 (2017)

38. Stroebel, D., Choquet, Y., Popot, J.-L., & Picot, D. An Atypical Haem in the Cytochrome B6F Complex. *Nature* **426**, 413-418 (2003).

39. Qin, X., Suga, M., Kuang, T., & Shen, J.R. Structural basis for energy transfer pathways in the plant PSI-LHCI supercomplex. *Science* **348**, 989-995 (2015).

40. MacGregor-Chatwin, C. *et al.* Lateral Segregation of Photosystem I in Cyanobacterial Thylakoids. *Plant Cell* **29**, 1119–1136 (2017).

41. Fotiadis, D., *et al.* Surface analysis of the photosystem I complex by electron and atomic force microscopy. *J. Mol. Biol.* **283**, 83–94 (1998).

42. Zhou, A. *et al*. Structure and Conformational States of the Bovine Mitochondrial ATP Synthase by Cryo-EM. *Elife* **4**, e10180 (2015).

43. Semchonok, D. A, Li, M., Bruce, B. D., Oostergetel, G. T., & Boekema, E. J. Cryo-EM structure of a tetrameric cyanobacterial photosystem I complex reveals novel subunit interactions. *Biochim. Biophys. Acta* **1857**, 1619-1626 (2016).

44. Sathish Yadav KN *et al.* Supercomplexes of plant photosystem I with cytochrome b6f, light-harvesting complex II and NDH. *Biochim. Biophys. Acta* **1858**, 12-20. (2016).

45. Gustafsson, M.G., *et al.* Three- dimensional resolution doubling in wide-field fluorescence microscopy by structured illumination. *Biophys. J.* **9**, 4957–4970 (2008).

46. Kirchhoff, H. *et al.* Dynamic control of protein diffusion within the granal thylakoid lumen. *Proc. Nat. Acad. Sci. USA* **108,** 20248–20253 (2011).

47. Haehnel, W. Photosynthetic electron transport in higher plants. *Annu. Rev. Plant Physiol*. **35**, 659 – 693 (1984).

48. Joliot, P. & Johnson, G. Regulation of cyclic and linear electron flow in higher plants. *Proc. Nat. Acad. Sci. USA **108,*** 13317-13322 (2011).

49. Ruban, A.V. & Murchie, E.H. Assessing the photoprotective effectiveness of non-photochemical chlorophyll fluorescence quenching: a new approach. *Biochim Biophys Acta* **1817**, 977–982 (2012)

50. Tikkanen, M., Grieco, M., Kangasjärvi, S. & Aro, E.M. Thylakoid protein phosphorylation in higher plant chloroplasts optimizes electron transfer under fluctuating light. *Plant Physiology* **152,** 723–735 (2010).

51. Kouril, R., *et al.* Structural characterization of a complex of photosystem I and light-harvesting complex II of *Arabidopsis thaliana*. *Biochemistry* **44,** 10935–10940 (2005).

52. Bell, A. J., Frankel, L. K. & Bricker, T. M. High yield non-detergent isolation of photosystem I-light harvesting chlorophyll II membranes from spinach thylakoids. *J. Biol. Chem.* **290**, 18429–18437 (2015).

53. Bos, I. *et al.* Multiple LHCII antennae can transfer energy efficiently to a single Photosystem I. *Biochim Biophys Acta* **1858**, 371-378 (2017).

54. Belgio, E. et al. Economic photoprotection in photosystem II that retains a complete light-harvesting system with slow energy traps. *Nature Comm*. **5**, 4433 (2014)

55. Johnson, M. P. *et al.* Photoprotective energy dissipation involves the reorganization of photosystem II light harvesting complexes in the grana membranes of spinach chloroplasts. *Plant Cell* **23,** 1468–1479 (2011).

56. Belgio, E., Ungerer, P. & Ruban, A. V. Light harvesting superstructures of green plant chloroplasts lacking photosystems. *Plant Cell Env.* **38,** 2035-2047 (2015).

57. Furbank, R.T., & Horton, P. Regulation of photosynthesis in isolated barley protoplasts: the contribution of cyclic photophosphorylation. *Biochim. Biophys. Acta* **894**, 332-338 (1987).

58. Miyake, C., Miyata, M., Shinzaki, Y. & Tomizawa, K. CO_2 response of cyclic electron flow around PSI (CEF-PSI) in tobacco leaves—relative electron fluxes through PSI and PSII determine the magnitude of non-photochemical quenching (NPQ) of Chl fluorescence. *Plant Cell Physiol.* **46**, 629–637.

59. Albertsson, P.Å., Andreasson, E., Stefansson, H., & Wollenberger, L. Fractionation of the thylakoid membrane. *Methods Enzymol.* **228**, 469–482 (1994).

60. Melis, A. Kinetic analysis of P700 photoconversion: effect of secondary electron donation and plastocyanin inhibition. *Arch. Biochem. Biophys*. **217**, 536–545 (1982).

61. Sanderson D, Anderson L, Gross E. Determination of the redox potential and diffusion coefficient of the protein plastocyanin using optically transparent filar electrodes. *Biochim. Biophys. Acta*. **852**. 269-278. (1987).

62. Blackwell, M. F., Gibas, C., Gygax, S., Roman, D. & Wagner B. The plastoquinone diffusion coefficient in chloroplasts and its mechanistic implications. *Biochim. Biophys. Acta.* **1183,** 533–543 (1994).

63. Danielsson, R., Albertsson, P. Å., Mamedov, F. & Styring, S. Quantification of photosystem I and II in different parts of the thylakoid membrane from spinach. *Biochim. Biophys. Acta* **1608,** 53–61 (2004).

64. Pribil, M., Labs, M., & Leister, D. Structure and dynamics of thylakoids in land plants. *J. Exp. Bot***. 5,** 1955-1972 (2014)

Author Information Correspondence and requests for material should be sent to M.P.J. (matt.johnson@sheffield.ac.uk).

Acknowledgements

We wish to thank Professor Peter Horton FRS (University of Sheffield) and Professor Francis-André Wollman (CNRS, Paris) for fruitful discussions on the manuscript. We also thank Professor Sir John Walker FRS (University of Cambridge) for providing samples of the bovine ATP synthase complex, Dr Erik Murchie (University of Nottingham) for loan of the Dual-PAM and Dr Chris Hill (University of Sheffield) for assistance with the EM. M.P.J. acknowledges funding from the Biotechnology and Biological Sciences Research Council (U.K.) grant BB/M000265/1, Leverhulme Trust grant RPG-2016-161, the Krebs Institute, Grantham Centre for Sustainable Futures and the Kirkwood Memorial Fund. CNH acknowledges the Photosynthetic Antenna Research Center (PARC), an Energy Frontier Research Center funded by the US Department of Energy, Office of Science, and Office of Basic Energy Sciences under Award Number DE-SC0001035. PARC's role was to partially fund the Multimode VIII AFM system and to provide partial support for C.N.H. The SIM imaging was performed at the University of Sheffield Wolfson Light Microscopy Facility and was partly funded by MRC Grant MR/K015753/1.

Author contributions W.W., C.M.C and M.J. performed the purification of membranes and characterised them by AFM. W.W and M.J. performed the spectroscopy experiments. W.W performed the EM

experiments. W.W. performed the AFM, EM and spectroscopy data analysis, figure preparation and Monte Carlo simulations. G.E.M. assisted with the modelling. S.F.H.B. performed the 3D-SIM experiments and data analysis. X.H. performed the AFM experiments on purified ATP synthase. J.H. provided advice and support to the AFM experiments. The work was conceived and written by M.P.J, and C.N.H. All authors discussed the results and commented upon the manuscript.

Figure Legends

Figure 1 | Biochemical and spectroscopic analysis of dark and growth light adapted thylakoids. a. SDS-PAGE analysis of proteins in dark thylakoids (TD), light thylakoids (TL), dark grana (GD), light grana (GL), dark stromal lamellae (SD) and light stromal lamellae (SL). **b.** Pro-Q Diamond phosphoprotein stain of SDS-PAGE samples in a. and Anti-PetC immunoblot revealing the cytochrome b_6f content of each sample. **c.** 77K fluorescence emission spectra of light (red) and dark (blue) thylakoids using 435 nm excitation. **d.** 77K PSI fluorescence excitation spectra of light (red) and dark (blue) thylakoids detected at 735 nm. **e.** 77K PSII fluorescence excitation spectra of light (red) and dark (blue) thylakoids detected at 700 nm. **f.** Absorption spectra of dark grana (solid blue line), light grana (solid red line), dark stromal lamellae (dashed blue line) and light stromal lamellae (dashed red line) samples. **g.** BN-PAGE analysis of protein complexes present in dark grana (GD), light grana (GL), dark stromal lamellae (SD) and light stromal lamellae (SL) samples.

Figure 2 | Macromolecular organisation of grana thylakoids. a. AFM topographs of dark-adapted grana thylakoids (scale bar: 100 nm). **b.** AFM topographs of light-adapted grana thylakoids (scale bar: 100 nm). **c.** Height cross-sections of the grana thylakoids in the main panels of (a) and (b) as shown by dashed lines. **d.** Histogram of the protein protrusion heights above the grana membrane surface with two-Gaussian fit in dark-adapted grana (blue line, N=121) and light-adapted grana (red line, N=126). **e.** Schematic model of measured protrusion heights in comparison with the atomic structures (PDBs: 1Q90 and 3JCU). **f.** Nearest neighbour analysis of the protein protrusions in dark-adapted grana (blue line, N=292) and light-adapted grana (red line, N=347) (**** Unpaired t-test. P <0.0001).

Figure 3 | Macromolecular organisation of stromal lamellae thylakoids. a. AFM topographs of dark-adapted stromal lamellae thylakoids (scale bar: 100 nm). **b.** AFM topographs of light-adapted stromal lamellae thylakoids (scale bar: 100 nm). **c.** Height cross-sections of the stromal lamellae thylakoids shown in the main panels in (a) and (b) by dashed lines. **d.** Histogram of the protein protrusion heights above the stromal lamellae membrane surface with two-Gaussian fit in dark-adapted stromal lamellae (blue line, N=227) and light-adapted stromal lamellae (red line, N=150). **e.** Schematic model of measured protrusion heights in comparison with the atomic structures (PDBs: 4Y28, 1Q90 and 5ARA). **f.** Nearest neighbour analysis of the protein protrusions in dark-adapted stromal lamellae (blue line, N=462) and light-adapted stromal lamellae (red line, N=298) (*Kolmogorov-Smirnov test. P=0.025).

Figure 4 | Dimerisation of PSI-LHCI supercomplexes in stromal lamellae thylakoids. a. AFM topographs of dark- and light-adapted stromal lamellae thylakoids showing putative PSI-LHCI dimers indicated by white ellipses (scale bar: 100 nm). **b.** Height cross sections of a representative PSI-LHCI dimer with average inter-complex distance (N=97). **c-e.** Possible arrangements of PSI-LHCI dimers modelled in Pymol (PDB: 4Y28), with contacts between PsaH and PsaB (c), PsaB and Lhca2 (d), and between Lhca2 and Lhca4 (e). Green colour indicates isoleucine 29 of PsaC which was used as a reference point for measurements. PSI-LHCII particles in AFM topographs which had nearest neighbours <14 nm exclude the contacts shown in (d) and (e) but not in (c).

Figure 5 | Membrane architectural changes. a. 3D-SIM of intact chloroplasts from dark- and light-adapted leaves showing six consecutive 125 nm optical slices through a chloroplast (scale bar: 1μm). **b**. full width at half maximum fluorescence intensity of the fluorescent spots (grana) in 3D-SIM images of intact chloroplasts from dark- (N=239) and light- (N=239) adapted leaves. (**** t-test. P<0.0001) **c.** Grana stacks per chloroplast in 3D-SIM images of intact chloroplasts from dark- (N=10) and light- (N=10) adapted leaves (** t-test. P=0.0073). **d.** thin-section EM image of a chloroplast within a dark-adapted leaf (scale bar: 0.5 μm). **e.** Thin-section EM image of a chloroplast within a light-adapted leaf (scale bar 0.5 μm). **f.** number of membrane layers per grana stack calculated from EM images of chloroplasts in dark (N=97) and light (N=96) adapted leaves (**** t-test (Welsch's correction for unequal variance). P<0.0001). **g.** 3D-SIM image of a chloroplast from Light/Dark-NaF treated leaves (scale bar: 1μm). **h.** 3D-SIM image of a chloroplast from Light/Dark+NaF treated leaves (scale bar: 1μm). **i.** full width at half maximum fluorescence intensity of the fluorescent spots (grana) in 3D-SIM images of intact chloroplasts from Light/Dark-NaF (N=200) and Light/Dark+NaF (N=200) treated leaves (**** t-test. P<0.0001).

Figure 6 | Changes in electron transfer and photoprotection. a. Model used for the Monte Carlo simulation based on AFM and EM/SIM data showing organisation of protein complexes (left) and thylakoid/lumen dimensions (right) (scale bar, 100 nm), see Methods for full explanation. **b**. Monte Carlo simulation of PC diffusion time from grana cytb_6f to stromal lamellae PSI modelled on light (red, N=4000) and dark-adapted (blue, N=4000) membrane organisation (mono-exponential association fit. k= 0.006, 0.008 for dark and light respectively). **c**. Monte Carlo simulation of PQH_2 diffusion time from grana PSII to stromal lamellae cytb_6f modelled on light (red, N=1000) and dark-adapted (blue, N=1000) membrane organisation (double-exponential decay fit. k_1 = 0.0028, 0.0007, k_2 = 0.0018, 0.0006, percent of fast component (relative amplitude of k_1) = 35%, 63%, for dark and light respectively). **d**. $P700^+$ reduction kinetics following a 250 ms saturating light pulse in light (red, N=4) and dark-adapted (blue, N=4) leaves in presence of MV. **e**. $P700^+$ reduction kinetics following a 250 ms saturating light pulse in Light/Dark+NaF (red, N=4) and Light/Dark-NaF (blue, N=4) leaves in presence of MV. **f**. $P700^+$ reduction kinetics following 20 s far-red light in light (red, N=14) and dark-adapted (blue, N=13) leaves (mono-exponential decay fit. k=1.101, 0.443 for dark and light adapted leaves respectively). **g**. $P700^+$ reduction kinetics following 20 s far-red light in Light/Dark+NaF (red, N=4) and Light/Dark-NaF (blue, N=4) leaves (mono-exponential decay fit. k=0.977, 0.711 for Light/Dark-NaF and Light/Dark+NaF treated leaves respectively). **h**. Transient NPQ generated by illumination of dark, light, Light/Dark+NaF and Light/Dark-NaF leaves (N=5 for each) with 200 μmol photons m^{-2} s^{-1} light for 5 mins followed by 3 mins dark. **i**. Changes in qP generated by illumination of dark, light, Light/Dark+NaF and Light/Dark-NaF leaves (N=5 for each) with 200 μmol photons m^{-2} s^{-1} light for 5 mins followed by 3 mins dark. **j**. PSII fluorescence induction in light (red, N=5) and dark-adapted (blue, N=5) leaves in the presence of DBIMB to monitor PQ reduction via a continuous illumination of limiting intensity. **h**. PSII fluorescence induction Light/Dark+NaF (red, N=5) and Light/Dark-NaF (blue, N=5) leaves in the presence of DBIMB to monitor PQ reduction via a continuous illumination of limiting intensity.

Figure 7 | Schematic model of the influence of grana stacking on the balance between LET and CET. a. Under moderate light, high levels of LHCII phosphorylation weaken LHCII-LHCII interactions resulting in more numerous smaller grana, creating a larger area of contact between the grana membranes (light green) and stromal lamellae/ grana end membranes (dark green). Under these conditions the diffusion of PC and PQ between grana and stromal lamellae is relatively fast, engaging cytb_6f in both domains efficiently in LET which predominates over CET. b. Under dark, low light and high light conditions dephosphorylation of LHCII strengthens LHCII-LHCII interactions resulting in fewer larger grana, reducing the area of contact between the grana membranes (light green) and stromal lamellae/ grana end membranes (dark green). Under these conditions the diffusion of PC and PQ between grana and stromal lamellae is relatively slow, leaving the stromal lamellae PQ pool in a more oxidised state that promotes efficient CET.

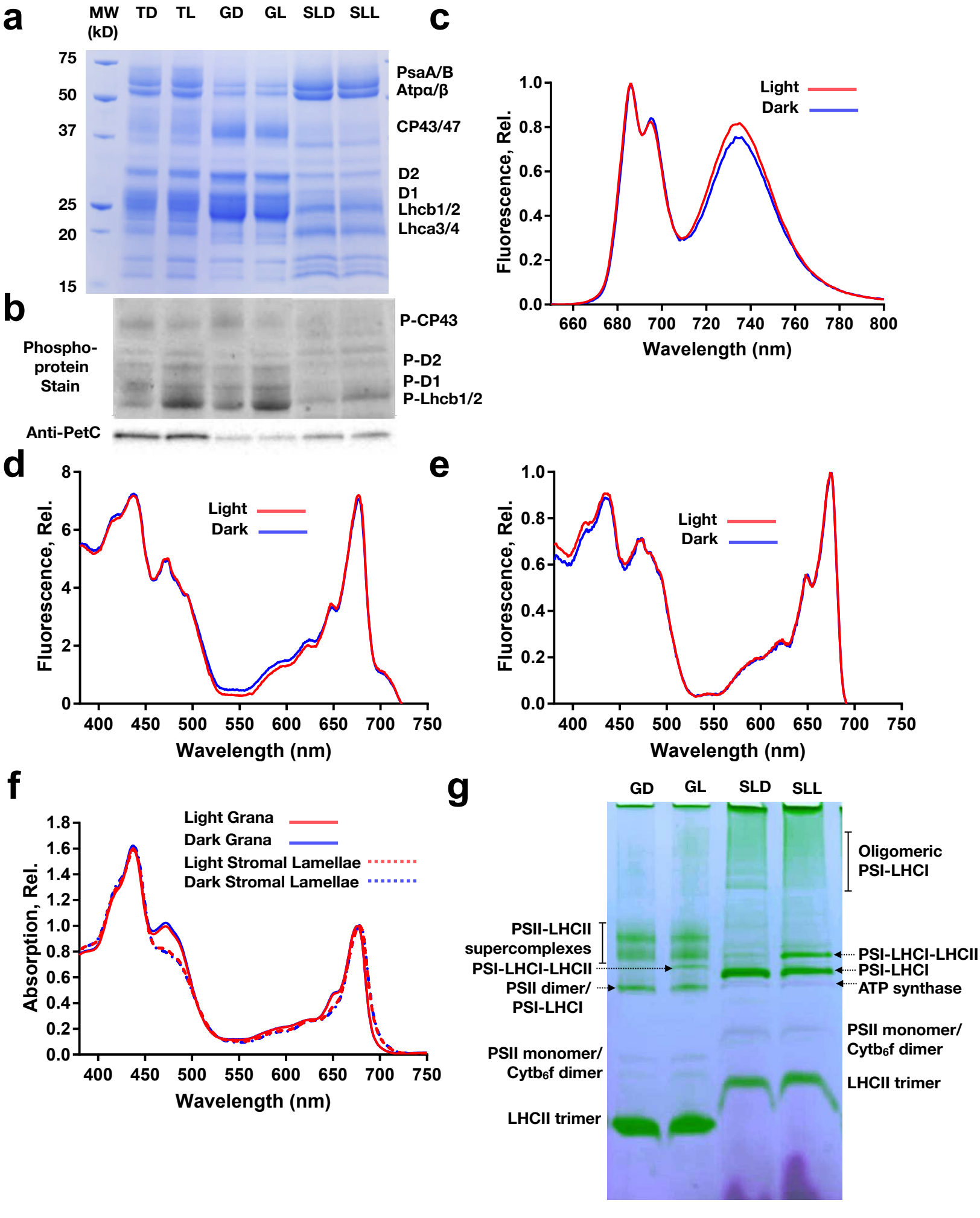
a
MW (kD)
TD
TL
GD
GL
SLD
SLL
75
50
37
25
20
15
PsaA/B
Atpα/β
CP43/47
D2
D1
Lhcb1/2
Lhca3/4
b
Phospho-protein Stain
P-CP43
P-D2
P-D1
P-Lhcb1/2
Anti-PetC
c
Light
Dark
Fluorescence, Rel.
Wavelength (nm)
d
Light
Dark
Fluorescence, Rel.
Wavelength (nm)
e
Light
Dark
Fluorescence, Rel.
Wavelength (nm)
f
Light Grana
Dark Grana
Light Stromal Lamellae
Dark Stromal Lamellae
Absorption, Rel.
Wavelength (nm)
g
GD
GL
SLD
SLL
Oligomeric PSI-LHCI
PSII-LHCII supercomplexes
PSI-LHCI-LHCII
PSII dimer/ PSI-LHCI
PSII monomer/ Cytb6f dimer
LHCII trimer
PSI-LHCI-LHCII
PSI-LHCI
ATP synthase
PSII monomer/ Cytb6f dimer
LHCII trimer

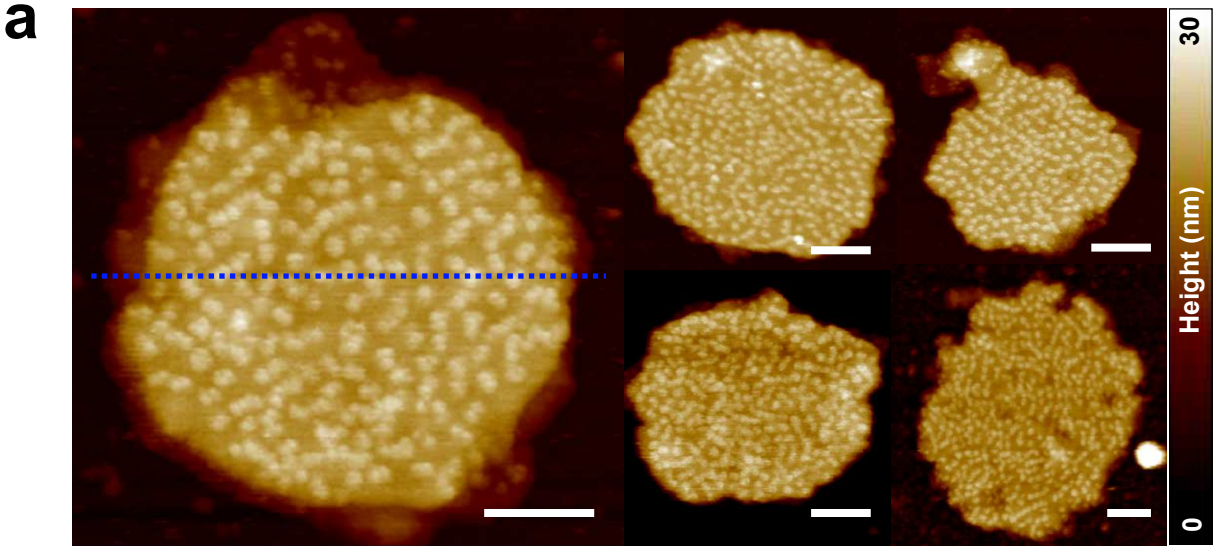
a
30
Height (nm)
0

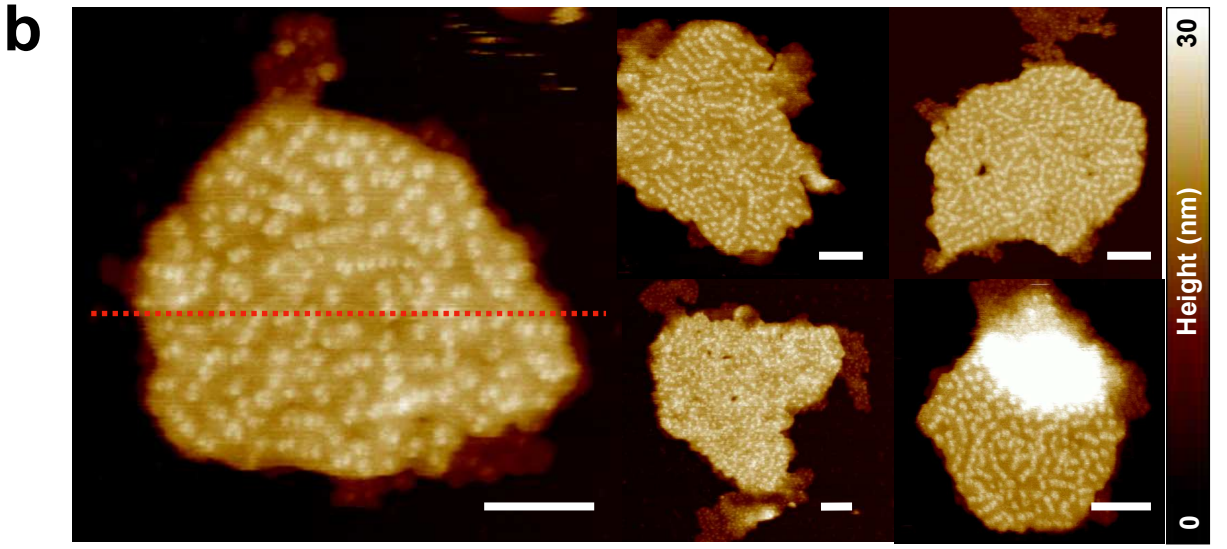
b
30
Height (nm)
0

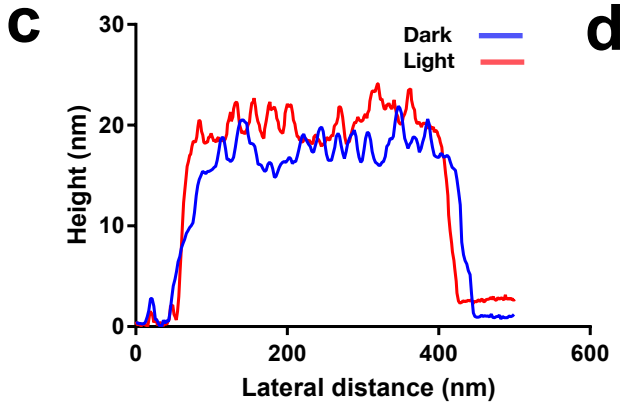
c
Dark
Light
Height (nm)
30
20
10
0
0
200
400
600
Lateral distance (nm)

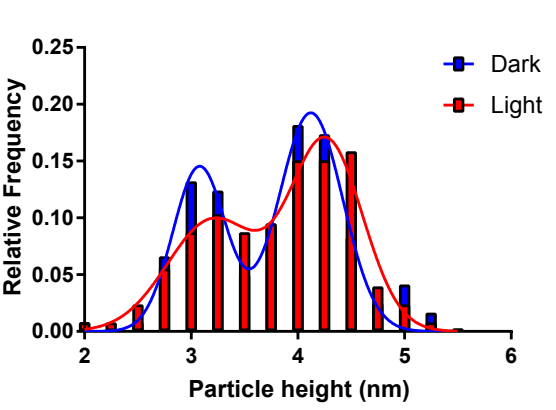
d
Dark
Light
Relative Frequency
0.25
0.20
0.15
0.10
0.05
0.00
2
3
4
5
6
Particle height (nm)

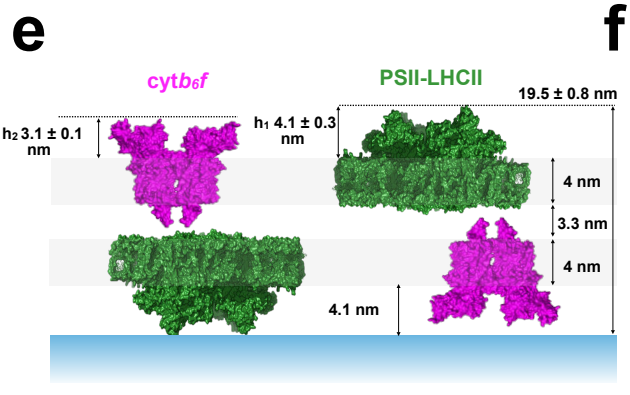
e
cytb6f
PSII-LHCII
19.5 ± 0.8 nm
h2 3.1 ± 0.1 nm
h1 4.1 ± 0.3 nm
4 nm
3.3 nm
4 nm
4.1 nm

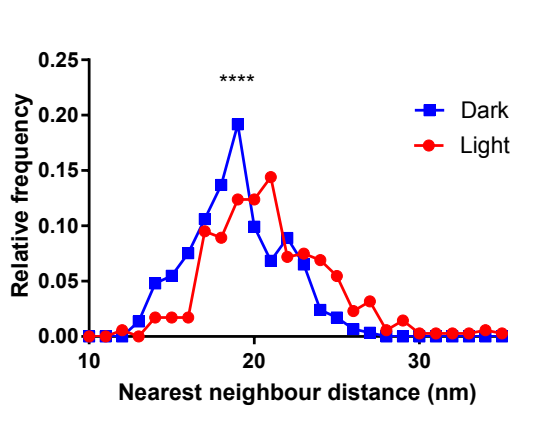
f
****
Dark
Light
Relative frequency
0.25
0.20
0.15
0.10
0.05
0.00
10
20
30
Nearest neighbour distance (nm)

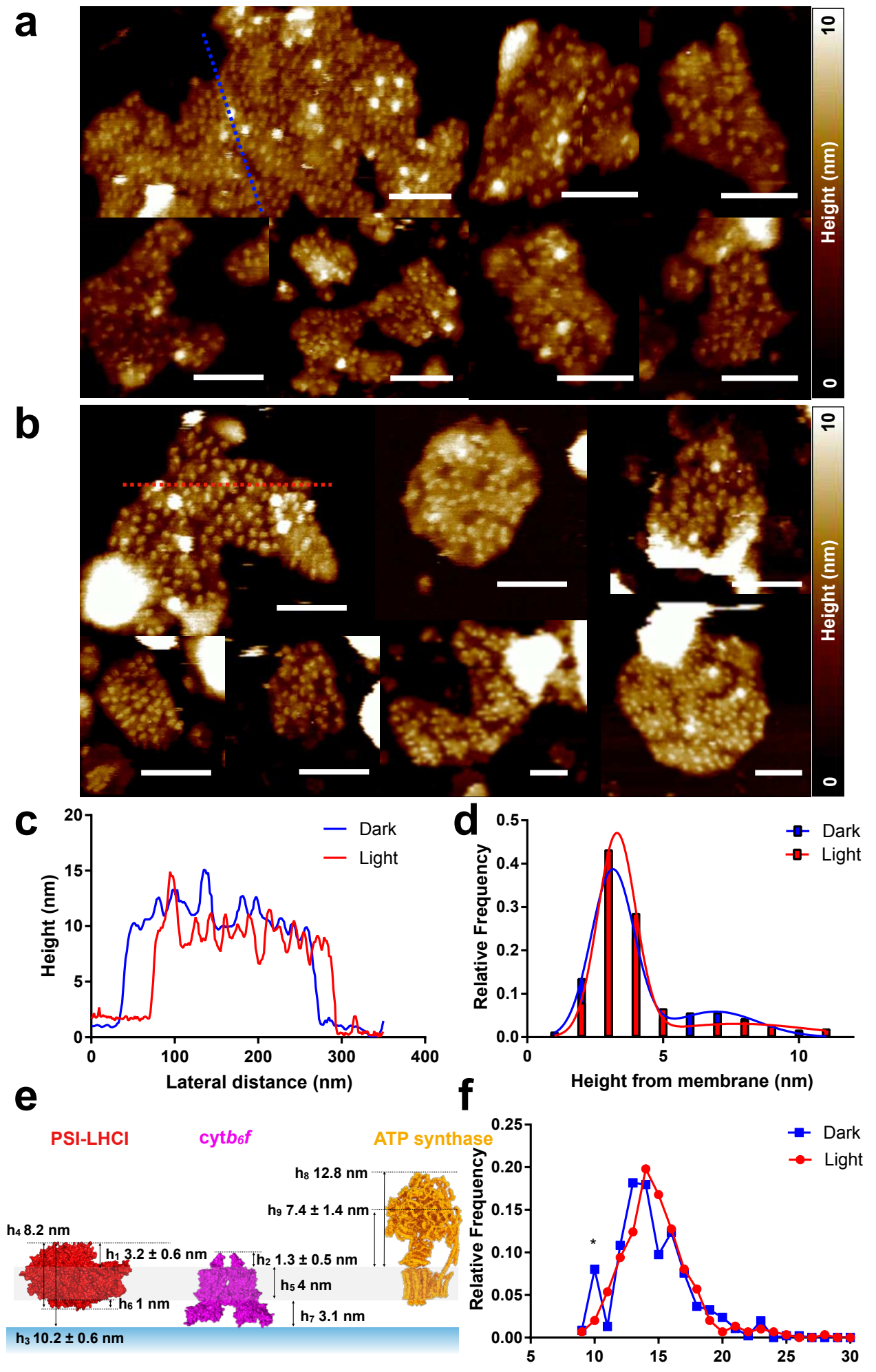
a
b
10
Height (nm)
0
c
Height (nm)
Lateral distance (nm)
Dark
Light
d
Relative Frequency
Height from membrane (nm)
Dark
Light
e
PSI-LHCI
cytb6f
ATP synthase
h8 12.8 nm
h9 7.4 ± 1.4 nm
h4 8.2 nm
h1 3.2 ± 0.6 nm
h2 1.3 ± 0.5 nm
h5 4 nm
h6 1 nm
h7 3.1 nm
h3 10.2 ± 0.6 nm
f
Relative Frequency
Nearest neighbour distance (nm)
Dark
Light
*

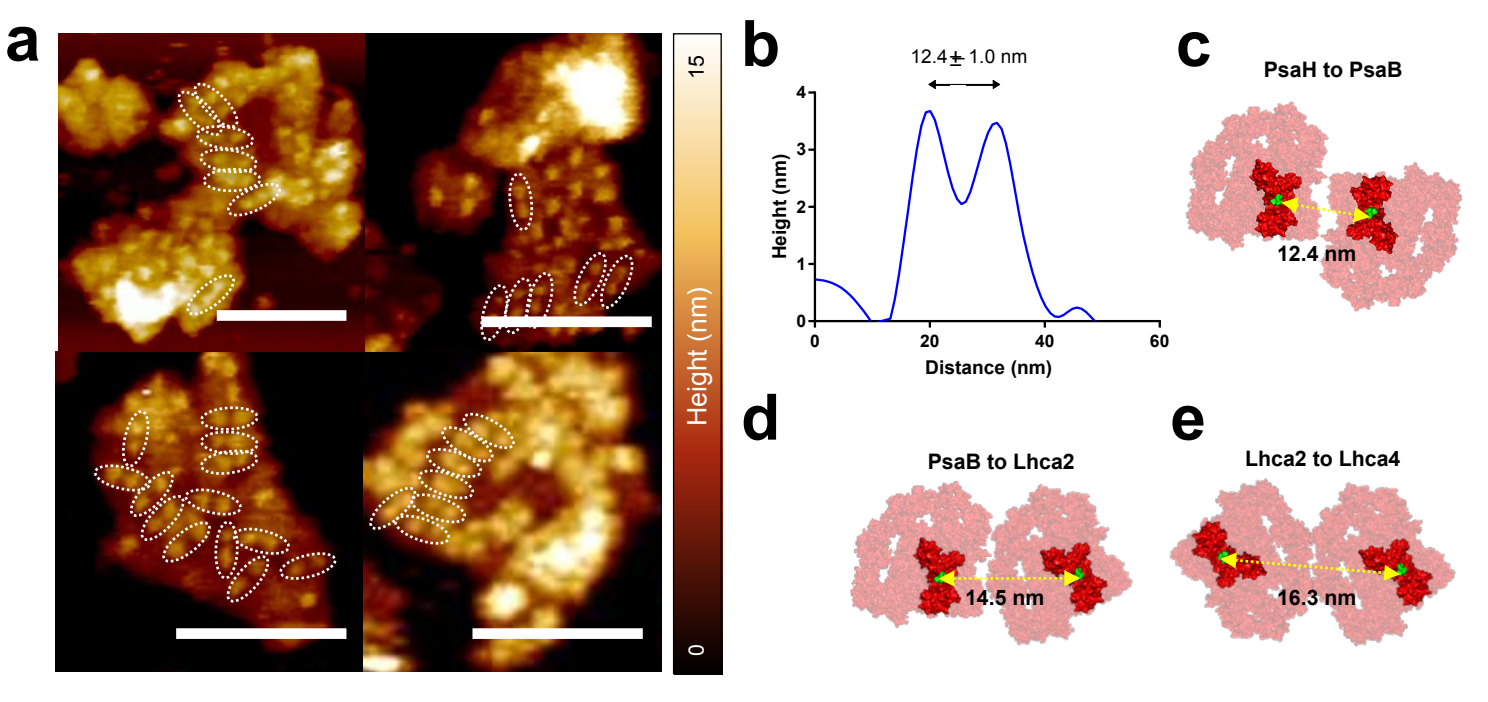
a
15
Height (nm)
0
b
12.4 ± 1.0 nm
Height (nm)
4
3
2
1
0
0
20
40
60
Distance (nm)
c
PsaH to PsaB
12.4 nm
d
PsaB to Lhca2
14.5 nm
e
Lhca2 to Lhca4
16.3 nm

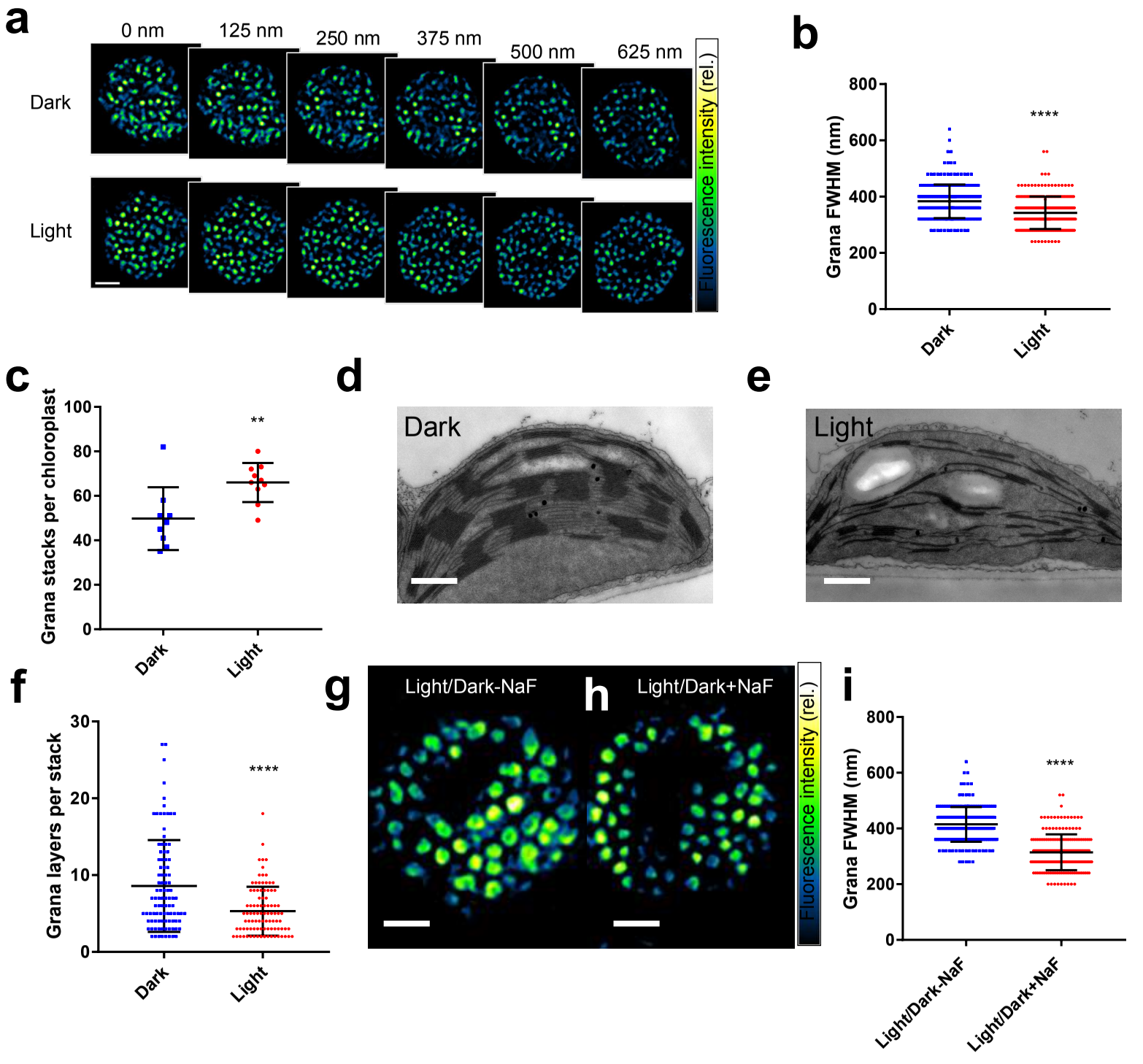
a
0 nm
125 nm
250 nm
375 nm
500 nm
625 nm
Dark
Light
Fluorescence intensity (rel.)
b
Grana FWHM (nm)
800
600
400
200
0
****
Dark
Light
c
Grana stacks per chloroplast
100
80
60
40
20
0
**
Dark
Light
d
Dark
e
Light
f
Grana layers per stack
30
20
10
0
****
Dark
Light
g
Light/Dark-NaF
h
Light/Dark+NaF
Fluorescence intensity (rel.)
i
Grana FWHM (nm)
800
600
400
200
0
****
Light/Dark-NaF
Light/Dark+NaF

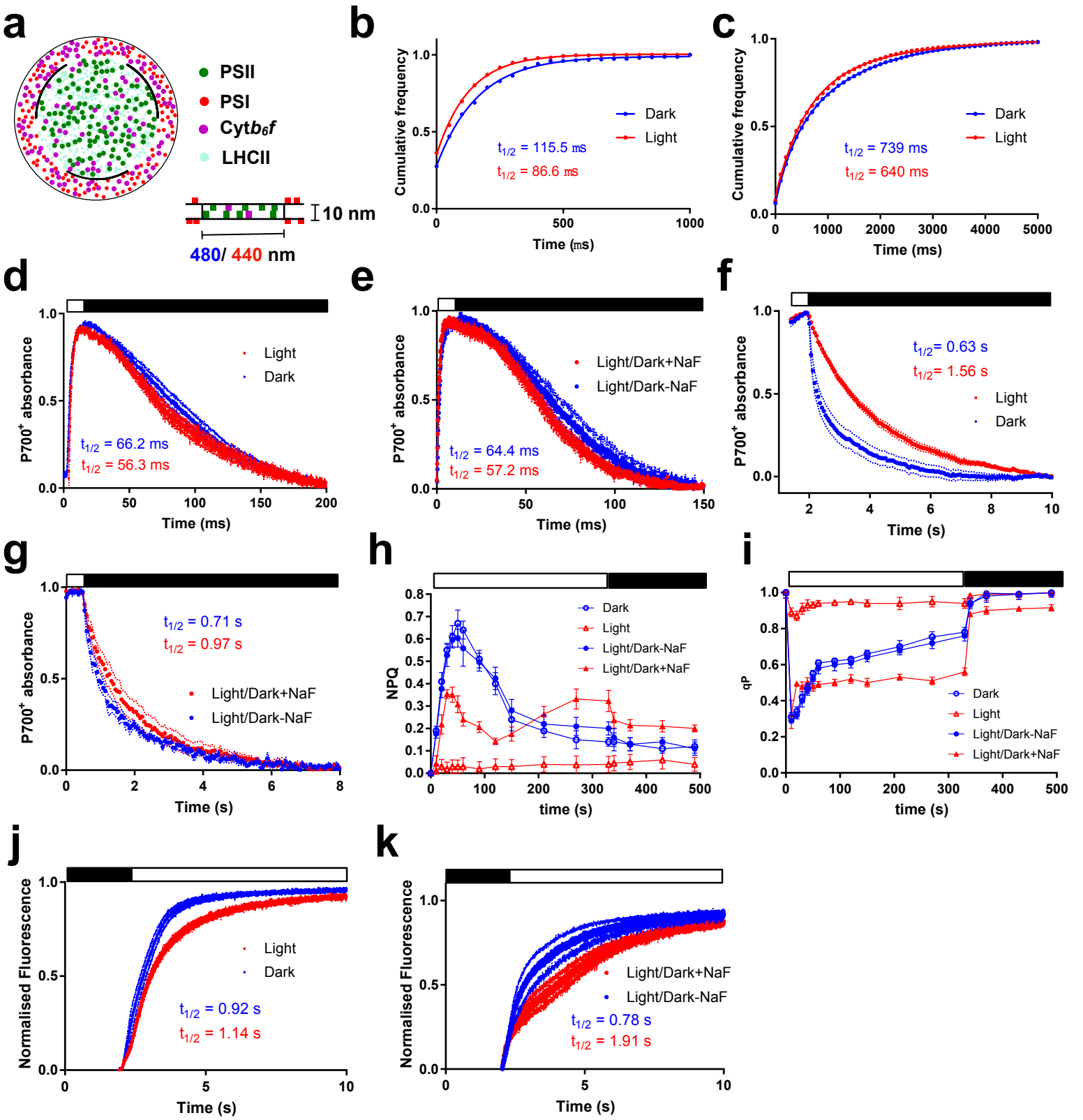
a
PSII
PSI
Cytb6f
LHCII
10 nm
480/ 440 nm
b
Cumulative frequency
Dark
Light
t1/2 = 115.5 ms
t1/2 = 86.6 ms
Time (ms)
c
Cumulative frequency
Dark
Light
t1/2 = 739 ms
t1/2 = 640 ms
Time (ms)
d
P700+ absorbance
Light
Dark
t1/2 = 66.2 ms
t1/2 = 56.3 ms
Time (ms)
e
P700+ absorbance
Light/Dark+NaF
Light/Dark-NaF
t1/2 = 64.4 ms
t1/2 = 57.2 ms
Time (ms)
f
P700+ absorbance
t1/2= 0.63 s
t1/2= 1.56 s
Light
Dark
Time (s)
g
P700+ absorbance
t1/2 = 0.71 s
t1/2 = 0.97 s
Light/Dark+NaF
Light/Dark-NaF
Time (s)
h
NPQ
Dark
Light
Light/Dark-NaF
Light/Dark+NaF
time (s)
i
qP
Dark
Light
Light/Dark-NaF
Light/Dark+NaF
time (s)
j
Normalised Fluorescence
Light
Dark
t1/2 = 0.92 s
t1/2 = 1.14 s
Time (s)
k
Normalised Fluorescence
Light/Dark+NaF
Light/Dark-NaF
t1/2 = 0.78 s
t1/2 = 1.91 s
Time (s)

a

Moderate Light
High LHCII-P

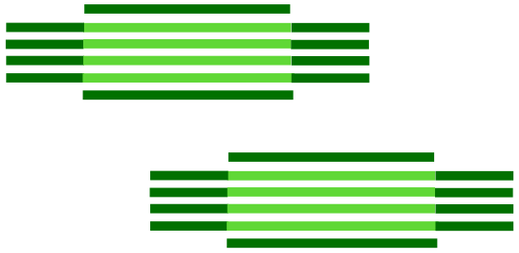

Small grana

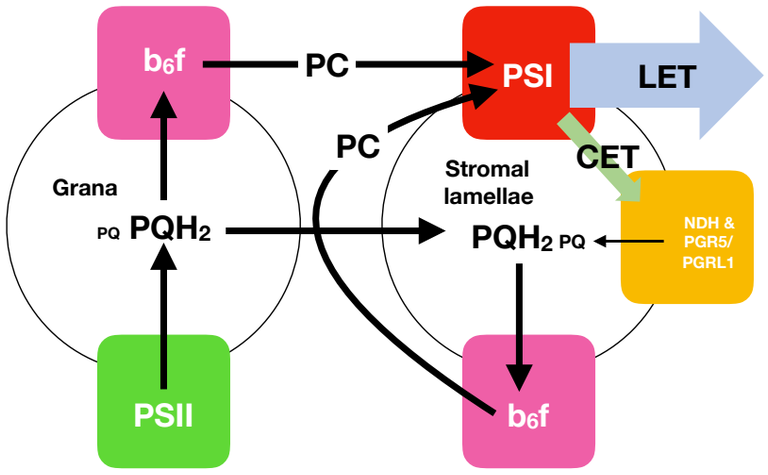

Reduced partition of grana and stromal lamellae PQ pools
LET enhanced

b

Dark/ Very low light/ High light
low LHCII-P

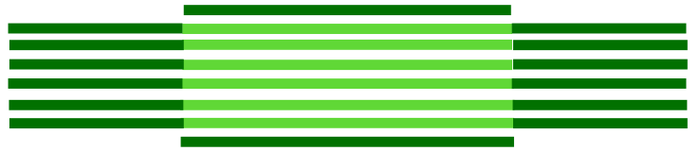

Large grana

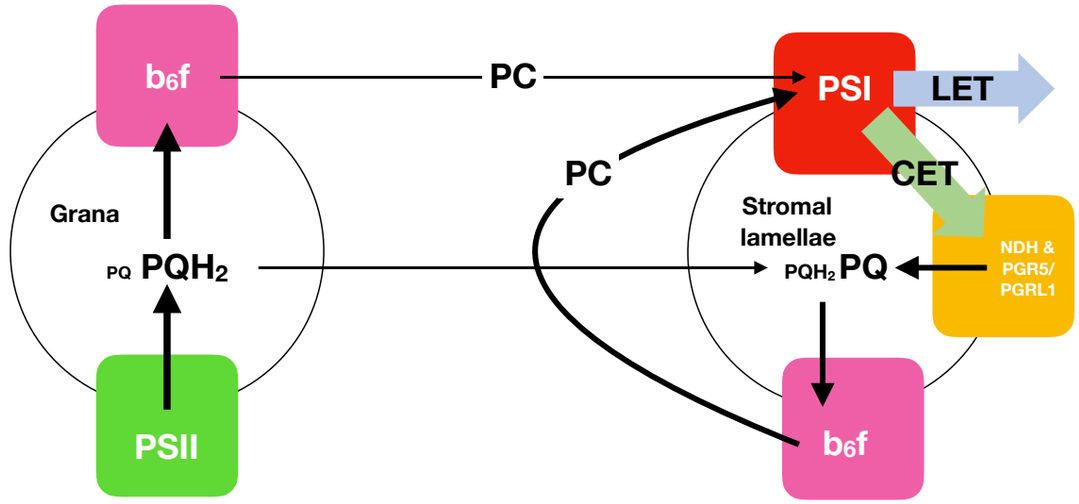

Increased partition of grana and stromal lamellae PQ pools
CET enhanced